Journal of
Water & Climate Change

IWA PUBLISHING

Journal of Water and Climate Change Vol 13 No 4, 1657 doi: 10.2166/wcc.2022.451

Evaluation of nonlinear dynamic patterns of extreme precipitation and temperatures in central England during 1931–2019

Farhang Rahmani* and Mohammad Hadi Fattahi

Department of Civil Engineering, Marvdasht Branch Islamic Azad University, Marvdasht, Iran
*Corresponding author. E-mail: farhang.rahmani@miau.ac.ir

FR, 0000-0001-8937-8701

ABSTRACT

Since climate change has altered extreme precipitation and temperature patterns, further study of these patterns is essential. The examination of precipitation and temperature patterns is of great significance to water engineers, water resources management, and hydrological studies. Accordingly, this study explored the nonlinear dynamic patterns and their sources governing extreme precipitation and temperatures using multifractal, shuffling, surrogating techniques, and extreme climate indices. The temperature and precipitation data regarding central England (1931–2019) were collected and used for analysis. The results of extreme climate indices demonstrated climate change in the study area. Besides, the multifractal analysis indicated that all indices' time series were characterized by multifractality. Despite the fact that multifractality of the maximum 1-day precipitation, minimum of maximum temperature, and maximum of maximum temperature was predominantly produced by correlation properties (long-range correlations between small and large local fluctuations), the multifractal characteristics of the warm nights were due to a probability density function (PDF) predominance. Moreover, multifractal properties of the diurnal temperature range, maximum 5-day precipitation, maximum of minimum temperature, minimum of minimum temperature, cool nights, and cool and warm days were produced by the identical extent of correlation properties and the PDF.

Key words: correlation, extreme climate indices, multifractal detrended fluctuation analysis (MF-DFA), multifractal source, shuffle, surrogate

HIGHLIGHTS

- Studying nonlinear dynamic patterns of temperatures and precipitation on a large scale.
- Using extreme climate indices for the evaluation of temperatures and precipitation.
- Employing MF-DFA to detect multifractal patterns in extreme temperatures and precipitation.
- Revealing multifractal sources using surrogate and shuffling techniques.

1. INTRODUCTION

In recent years, climate change has garnered attention as a serious concern for humanity. The investigation of extreme temperatures and precipitation offers insights into climate change as its consequences intensify anomalies in the hydrological cycles (Panthou *et al.* 2014; Agbazo *et al.* 2019). In conjunction with soaring temperatures, precipitation patterns have evolved so dramatically that the frequency and severity of extreme climatic events, including droughts and floods, has radically increased (Wang *et al.* 2016; Agbazo *et al.* 2019). The study of extreme climate phenomena has thus become indispensable. Extremes are describable by the highest and least values of climatic parameters (e.g., temperature and precipitation) that are likely to happen in a study area at a particular time (Vega & Rohli 2012). Extreme climate indices represent the extreme high and low precipitation and temperatures in an area and offer non-stationarity identification of extremes' intensity, frequency, and duration. Thus, extreme climate indices provide a more comprehensive and accurate view than the raw precipitation and temperature data. Accordingly, in this study, extreme climate indices were used to study the patterns of temperature variations at night and day, extreme temperatures, and significant precipitation. Extreme climate indices hitherto have been used in numerous studies, including the analysis of long-term shifts in the extreme climate indices of the Mediterranean by Abbasnia & Toros (2019) and the selection of climate change scenarios based on extreme climate indices by Seo *et al.* (2019). Besides these, spatiotemporal variations in extreme climate events in China were examined by Guo

et al. (2019) and non-stationary modeling was developed by Hao *et al.* (2019). Moreover, modeling for identifying hidden climate indices from occurrences of hydrologic extremes was done by Renard & Thyer (2019), global climate indices to study rainfall variabilities in southeast Asia were used by Singh & Qin (2020), and finally, investigation of causes of Parishan Lake drying was done by Rahmani & Fattahi (2021c) using the phase-space reconstruction technique, a drought index, and extreme climate indices.

The UK has been hit by several extreme climatic phenomena in recent decades, including successive heat waves, cold waves, droughts, and floods. According to the Met Office website (the national meteorological service for the UK), the UK witnessed a severe cold winter in 2009–2010, which was unprecedented since 1987. This cold wave swept across Europe. The cold wave in the UK led to considerable financial and human losses. Another extreme cold wave was also recorded the following year (2010–2011), breaking the record of low temperature in the UK from 1981 until then, which caused heavy snowfalls and triggered serious transportation problems across the country. In the spring and summer of 2012, the UK experienced several floods and flash floods. Furthermore, in the fall of 2013, torrential rain and strong winds with a speed of 160 km per hour hit the UK. More flash floods, floods, and strong winds were recorded in December 2013, winter 2013–2014, winter 2015–2016, the autumn of 2017, the autumn and winter of 2019–2020, and July 2021. Extreme heat and cold waves were also recorded in 2013–2014 and 2018 (for further details, see https://www.metoffice.gov.uk/). Moreover, the UK has suffered from various flooding events, including autumn and winter flooding in 1998, 2000, and 2001 (Marsh 2001; Wheater 2006), flash flooding in 2004 and 2007 (Doe 2004; Golding *et al.* 2005), and several droughts such as in 1975–1976, 1988–1992, 1995–1997, 2003, 2004–2006, 2010–2012, and 2018 (Holman *et al.* 2021). In the mentioned events, a vast area of central England (CE) was affected by extreme climatic phenomena, which in some cases brought about considerable damages. Since the UK is highly prone to experiencing extreme climatic phenomena (especially CE), a region in the UK was selected to study the nonlinear dynamic patterns of extreme temperatures and precipitation.

Several studies have been conducted to investigate the effects of extreme climatic phenomena (specifically floods and droughts) on the UK from various perspectives, such as Asadullah (2019), Parsons *et al.* (2019), Bryan *et al.* (2020), and Wallace (2022). Public and private organizations have also conducted studies on climate and climate change in the UK (Kendon *et al.* 2020). Some studies have specifically examined temperature variations in CE (Chapman *et al.* 2020; Shi *et al.* 2021; Haupt & Fritsch 2022). Nevertheless, none of these studies looked at the nonlinear dynamic patterns of extreme precipitation and temperatures. In addition to this, sources of the nonlinear dynamic patterns were not examined. It is essential to study the patterns of extreme precipitation and temperatures from the nonlinear dynamic point of view because non-dynamic and linear perspectives are not able to reveal the latent long-term mechanisms of extreme precipitation and temperatures. Scrutinizing nonlinear dynamic patterns of extreme precipitation and temperatures can expose the impact of climate change on the study area sufficiently and more effectively than other perspectives. A profound understanding of the hydrological time series offers a more manageable extremes prediction, which is essential for water resource management and risk assessment. Accordingly, the significance of this issue motivated this study. This study is of relevance for enhancing our understanding of nonlinear dynamic and multi-scale patterns of extreme precipitation and temperatures. It is of significance to climate change, water engineering, and hydrologic studies.

An accurate and efficient application is required to analyze and reveal nonlinear dynamic patterns governing climatic and hydrological phenomena. The multifractal theory is acknowledged as a proper technique for nonlinear dynamic patterns in time series. Mandelbrot (1982) was the first to use the fractal mathematical technique for measurements, and then the fractal method was additionally theorized and developed by Evertsz & Mandelbrot (1992), Brown *et al.* (1992), Olsen (1995), Riedi (1995), and Pesin (2008). Frisch & Parisi (1985) were the first to realize that chaotic phenomena could be composed of intermittent multifractal processes (Isaacson 2018). This discovery provided grounds for proposing multifractal analysis by Frisch & Parisi (1985). Multifractality is found in various phenomena (e.g., climate change, river flows (Hekmatzadeh *et al.* 2020), temperatures (Rahmani & Fattahi 2021a), and drought patterns (Rahmani & Fattahi 2021a)). A mono-fractal time series (signal) exhibits an identical regularity everywhere in time, and conversely, a multifractal signal (time series) depicts variations in signal regularity over time. Thus, this study applied multifractal theory to detect the essence of the existing patterns in the hydrological time series.

Distinct multifractal analysis techniques have been developed based on partition function multifractal formalism (Feder 1988) and standard multifractal analyses, such as the wavelet transform modulus maxima (WTMM) method (Muzy *et al.* 1991), detrended fluctuation analysis (DFA) (Peng *et al.* 1994), and multifractal detrended fluctuation analysis (MF-DFA) (Mandelbrot 1989). This has been conducted to overcome obstacles (e.g., time-series stationary and multi-scale analysis

problems) and calculate multifractal attributes. In the present study, the MF-DFA method is employed to estimate the multifractality characteristics of the time series which is going to be mentioned in the following sections.

To assess the multifractality in the time series of extreme climate indices and to evaluate extreme precipitation and temperatures nonlinear dynamic, first, 11 extreme climate indices (diurnal temperature range (DTR)), RX1day (maximum 1-day precipitation amount), RX5day (maximum 5-day precipitation amount), TXx (maximum Tmax), TNx (maximum Tmin), TXn (minimum Tmax), TNn (minimum Tmin), TN10p (cool nights), TX10p (cool days), TN90p (warm nights), and TX90p (warm days)) were employed to evaluate extreme precipitation and temperatures in the study area. Subsequently, multifractal, surrogating, and shuffling techniques were adopted to detect multifractal properties and multifractal sources in the time series.

Section 2 provides details regarding study areas and data sources. Section 3 presents theoretical details concerning multifractal analysis and extreme climate indices; then, in Section 4, the results and discussions are delivered. In the last section 5, a summary and conclusion to the research are presented.

2. STUDY AREA AND DATA SOURCES

The precipitation and temperature time series regarding CE were generated by Alexander & Jones (2001) and Parker *et al.* (1992). Parker *et al.* (1992) selected 11 stations to represent CE data (as detailed in Parker *et al.* (1992)). Since there were several gauging stations in the CE, stations that were highly urbanized or did not reflect the geographical properties of the area were not selected. For instance, gauging stations in frost-hollows, on the coast, and in uplands were ignored. Parker *et al.* (1992) used various techniques to modify and homogenize the data, such as variance, and correlation coefficients. The output data of Parker *et al.* has been validated and does not require statistical modifications. Thus, the data can be used for analysis and calculations without preprocessing. The series has since been updated, and it is now stored on the Met Office website (https://www.metoffice.gov.uk/hadobs/hadcet/data/download.html). Additionally, Alexander & Jones (2001) updated the precipitation series in the UK that data are also accessible through the Met Office (https://www.metoffice.gov.uk/hadobs/hadukp/). For their series, the UK was divided into nine districts (South-west, South-east, Central, North-west, North-east, Southern Scotland, Eastern Scotland, Northern Scotland, and Northern Ireland). To calculate extreme climate indices, precipitation and temperature data on a daily scale were collected from the Met Office website regarding CE from 1931 to 2019. The study region is shown in Figure 1. CE is roughly stretched from north to south between 53.4 and 51.2 N. It is also located from west to east between 2.5 W and 47.26 E. The average maximum temperature, minimum temperature, and precipitation in CE (between 1931 and 2019) are 13.95 °C, 6.22 °C, and 54.8 mm, respectively.

3. METHODOLOGY

3.1. Extreme climate indices

First, the extreme climate indices were determined, as shown in Table 1. Commonly, extreme climate indices refer to precipitation or temperatures, the measurements of which require daily precipitation data and maximum and minimum temperature data. Indices reveal events that could occur multiple times throughout the season or the year by suggesting strong statistical features instead of extreme measurement that extremes could not be witnessed throughout some years (Alexander *et al.* 2006). The extreme climate indices were used to study the patterns of temperature variations at night and day, extreme temperatures, and significant precipitation. The extreme indices are classified into five groups: (1) percentile-based; (2) absolute; (3) threshold; (4) duration; and (5) other indices, including annual precipitation total (PRCPTOT), DTR, simple daily intensity index (SDII), extreme temperature range (ETR), and annual contribution from very wet days (R95pT) (Alexander *et al.* 2006). This study employed four percentile-based indices (TN10p, TN90p, TX10p, and TX90p), six absolute indices (RX1day, RX5day, TNn, TNx, TXx, and TXn), and DTR indices (see Table 1). To calculate extreme climate indices, an R code was employed. R code is accessible to everyone through the following link: https://github.com/ECCC-CDAS/RClimDex, and details are in https://cran.r-project.org/web/packages/climdex.pcic/climdex.pcic.pdf.

3.2. Multifractal detrended fluctuation analysis (MF-DFA)

The MF-DFA is a well-known application for determining mono-fractal scaling characteristics and exploring long-range correlations in noisy, non-sub-basinary time series, which is very common in hydrological phenomena (Kantelhardt *et al.* 2002). The MF-DFA technique can be used for multifractality assessment in the time series, and its accurate results for non-sub-basinary series (Adarsh *et al.* 2020; Miloş *et al.* 2020) prove the proper functionality of this tool for finding multifractal

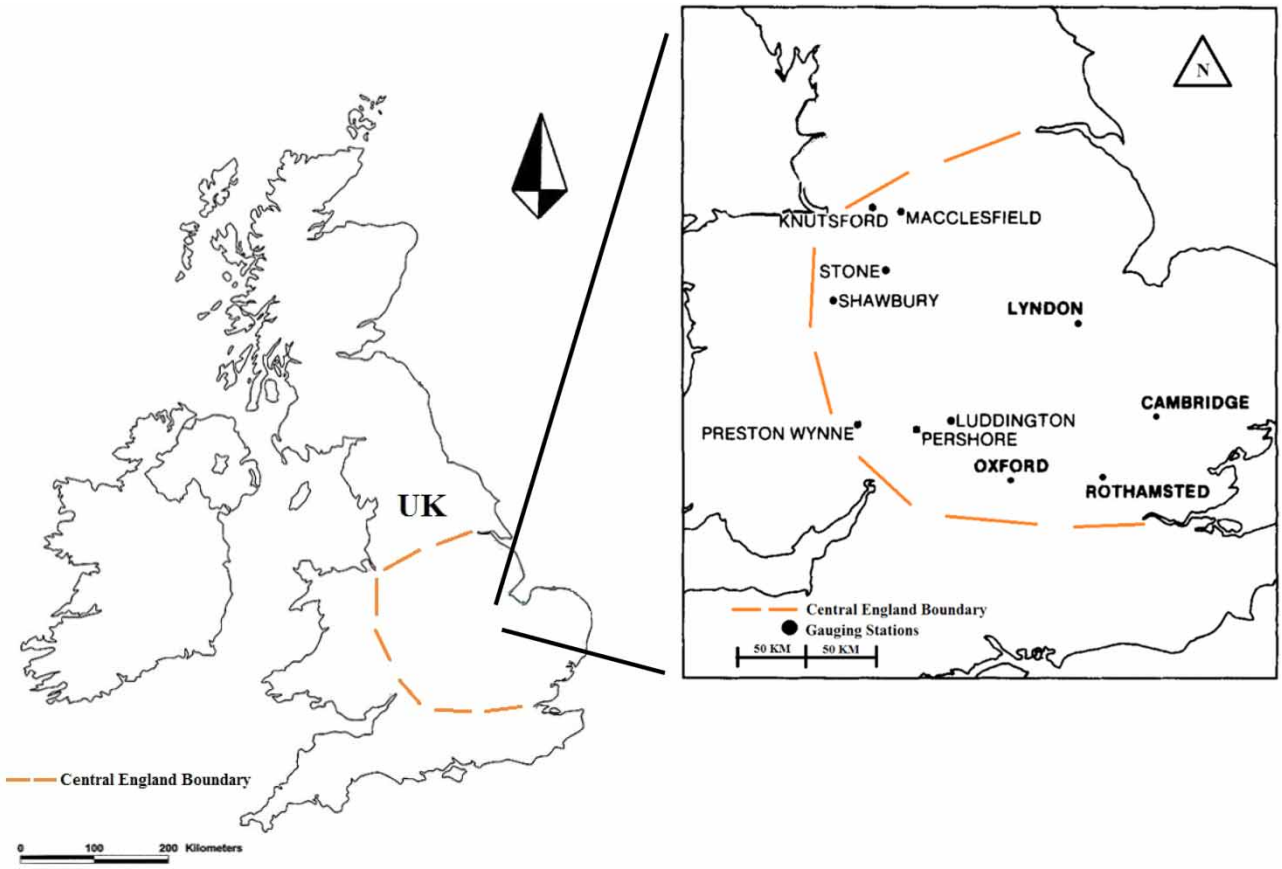

Figure 1 | CE's location (approximate boundary) in the UK and gauging stations.

Table 1 | Description of the selected extreme climate indices (available online at http://cccma.seos.uvic.ca/ETCCDI/list_27_indices.shtml)

ID	Indicator name	Definitions	Unit
RX1day	Maximum 1-day precipitation amount	The monthly maximum 1-day precipitation	mm
RX5day	Maximum 5-day precipitation amount	The monthly maximum of consecutive 5-day precipitation	mm
TN10p	Cool nights	Percentage of days when TN<10th percentile	Days
TN90p	Warm nights	Number of days when TN>90th percentile	Days
TX90p	Warm days	Percentage of days when TX>90th percentile	Days
TX10p	Cool days	Percentage of days when TX<10th percentile	Days
TXx	Maximum Tmax	Annual maximum value of daily maximum temperature	°C
TXn	Minimum Tmax	Annual minimum value of daily maximum temperature	°C
TNn	Minimum Tmin	Annual minimum value of daily minimum temperature	°C
TNx	Maximum Tmin	Annual maximum value of daily minimum temperature	°C
DTR	Diurnal temperature range	Annual mean difference between TX and TN	°C

patterns in the hydrological time series. Therefore, the MF-DFA technique was utilized to determine multifractal patterns in the time series. Five steps are required for the MF-DFA procedure (Mandelbrot *et al.* 1997; Movahed *et al.* 2006):

Step I: generating a profile $Y = \{y_\tau\}_{\tau=1}^{n}$ using Equation (1), where n is series length and y_τ is τth profile value.

Step II: dividing Y into non-overlapping segments $I_s = \text{int}(n/s)$ with equal length s.

Step III: variance determination based on each segment local trend estimated through an order n polynomial fit to the data (Equation (2)).

$$y_\tau = \sum_{k=1}^{\tau} (x_k - \bar{x}), \quad (\tau = 1,\ 2,\ \ldots,\ n) \tag{1}$$

$$F^2(\nu, s) = \frac{1}{s}\sum_{i=1}^{s} \{Y[(\nu-1)s + i] - y_\nu(i)\}^2 \quad , \quad \nu = 1,\ 2,\ \ldots,\ N_s \tag{2}$$

Regarding all segments ν, the best polynomial fit concerning $Y[(\nu-1)s+i]$ is shown by $y_\nu(i)$.

Step IV: Calculating the mean variance for all segments using Equation (3):

$$\begin{cases} F_q(s) = \left\{\frac{1}{N_s}\sum_{\nu=1}^{N_s} [F^2(\nu, s)]^{\frac{q}{2}}\right\}^{\frac{1}{q}}, & q \neq 0 \\ F_0(s) = \exp\left\{\frac{1}{2N_s}\sum_{\nu=1}^{N_s} \ln F^2(\nu, s)\right\}, & q = 0 \end{cases} \tag{3}$$

Step V: According to power law, the association between $F_q(s)$ and scale s is defined by Equation (4):

$$F_q(s) \propto s^{H(q)} \tag{4}$$

To assess the fluctuation function scaling performance, the log–log plots of $F_q(s) \sim s$ for each q value are practical (Feder 1988). The scaling exponent $H(2)$ can be employed for the interpretation of the second-order properties of the time series (the positive or negative long-range power-law correlation in the time series). $0.5 < H(2) < 1$ shows a long-range correlation, whereas $0 < H < 0.5$ indicates a short-range correlation in the time series. The time-series mono-fractality can be implied through $H(q)$ values independent from q. Conversely, a time series is multifractal if $H(q)$ exhibits a dependency upon q values.

3.3. Multifractal strength analysis

The more multifractal patterns in the time series, the higher the multifractal strength of the time series. The values of the difference between the maximum singularity index and the minimum singularity index can be used to assess the multifractality (multifractal strength) of the time series. Higher values of this difference indicate a greater number of multifractal patterns in the time series. This difference is shown by $\Delta\alpha$. To estimate $\Delta\alpha$, first, the mass or multifractal scaling exponent $\tau(q)$ should be computed by Equation (5) (Kantelhardt *et al.* 2002):

$$\tau(q) = q \times H(q) - 1 \tag{5}$$

The mono-fractal time series represents itself with a linear curve in the $\tau(q) \sim q$ graph. However, a multifractal time series represents itself with a nonlinear curve in the $\tau(q) \sim q$ graph. The curves' nonlinearity extent verifies the multifractality; an increment in the nonlinearity is directly associated with more robust multifractality.

After $\tau(q)$ evaluation, the singularity spectrum $f(\alpha)$ is computed (Equation (6)). The $f(\alpha)$ values designate the time-series multifractal components. The multifractal strength of a time series can be denoted by $f(\alpha)$ width. When $f(\alpha)$ is a single point in the multifractal spectrum diagram, the time series is mono-fractal.

$$\alpha = \frac{\partial\tau(q)}{\partial q}, \quad f(\alpha) = \alpha q - \tau(q) \tag{6}$$

In Equation (6), α is the Hölder exponent (singularity index). The singularity index is used to measure the time-series singularity degree, indicating the fractality of the data points in a time series. Finally, $\Delta\alpha$ can be assessed by $f(\alpha)$ width, reflecting the distribution evenness and fractal strength in the time series. The higher the value of $\Delta\alpha((\alpha_{\max} - \alpha_{\min}))$, the higher the

multifractal strength of the time series. To evaluate multifractality in the time series, the primary MATLAB codes rendered by Espen Ihlen (2020) were utilized. For further details regarding multifractal analysis and multifractal sources, see Rahmani & Fattahi (2021b).

3.4. Multifractal source analysis

It is widely accepted that two types of multifractal sources can be found in a time series. The first is the long-range correlations between small and large fluctuations (correlation attributes) in the time series, and the second is a broad probability density function (PDF) (Liu *et al.* 2013; Rego *et al.* 2013). The two methods of shuffling and surrogating can be employed to assess the multifractal sources in the series. Using the shuffling method, the correlation in the time series is eliminated, and its impacts on the time series are examined. The surrogate method saves correlation properties in the time series; therefore, PDF impacts can be scrutinized.

Shuffling is a reliable method of distinguishing multifractal sources in a time series. Through shuffling, correlations are dropped, while fluctuation characteristics and PDF remain unaffected. The multifractal sources of a time series are deemed to be correlation attributes when the shuffled time series exhibits a random response ($H_{shu}(q)$ =0.5, where H is the generalized Hurst exponent). Likewise, if the multifractality is not destroyed by shuffling, then a PDF is the source of the multifractality. If the multifractal strength of the shuffled time series is less than that of the original, both PDF and correlation properties are multifractal origins (Rego *et al.* 2013).

Surrogate theory can be applied to evaluate the influence of the broadness of PDF. In the present study, Iterative Amplitude Adjusted Fourier Transform (IAAFT) was adopted to generate a surrogate time series (Schreiber & Schmitz 1996, 2000). The surrogate method does not influence the correlation properties of a time series. A surrogate time series is generated from the original by randomizing the phase of the time series in Fourier space, such that the surrogate series is Gaussian. Thus, if the $H_{surr}(q)$ independency of q is proven concerning the surrogated time series, then the multifractality of the series is the result of a broad PDF. By examining the components of the surrogate time series, one can determine the strength of PDF and correlation properties. If the multifractalities of both the shuffled and surrogated time series are weaker than those of the original time series, both correlation properties and PDF are the sources of its multifractality. The shuffling method is sufficient to investigate the multifractality source of the time series; however, by the surrogate method, more accurate results can be obtained concerning PDF influences.

The studies' results have shown that the q range [−10 to 10] is commonly proper for multifractal analysis; this range was selected in this study (Kantelhardt *et al.* 2003; Zhang *et al.* 2019). The time scale (s) was selected in the range $[2^3 \sim 2^{7.7}]$ (for all indices except DTR, TNx, TNn, TXn, and TXx; to avoid crossover scale, see (Ge & Leung 2013)) and $[2^3 \sim 2^{4.65}]$ (for DTR, TNx, TNn, TXn, and TXx).

The daily precipitation and daily maximum and minimum temperatures in the time series were used to define the extreme climate indices. Then, the time series of computed indices were assessed for multifractal characteristics using MF-DFA. This will reveal the multifractal patterns governing maximum 1-day precipitation amount, maximum 5-day precipitation amount, cool nights, warm nights, cool days, warm days, maximum Tmax, minimum Tmax, maximum Tmin, minimum Tmin, and DTR. The results are discussed in the next section. The methodology was presented in the form of a flowchart as shown in Figure 2.

4. RESULTS AND DISCUSSION

As shown in Figure 3, the values of extreme indices of warm days, warm nights, maximum Tmax, minimum Tmax, maximum Tmin, minimum Tmin, and DTR were escalated, and linear and cubic fit lines suggested an upward (positive) slope.

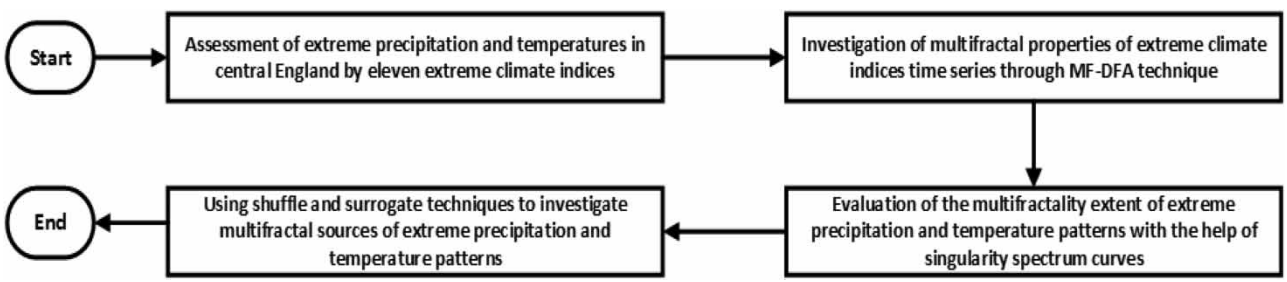

Figure 2 | A graphical illustration of the analysis steps.

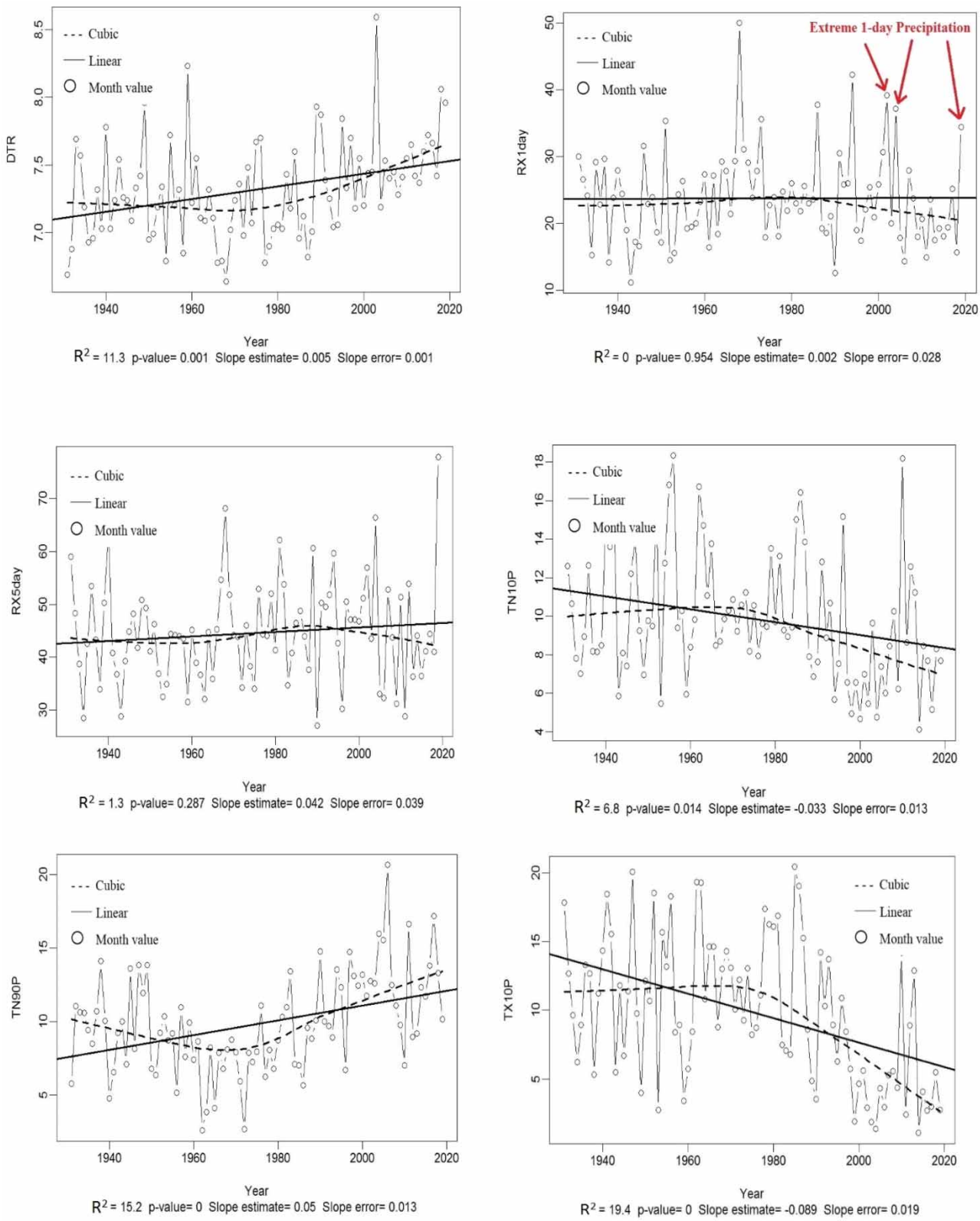

Figure 3 | Extreme climate indices and cubic and linear fit lines concerning CE from 1931 to 2019. (*continued*.).

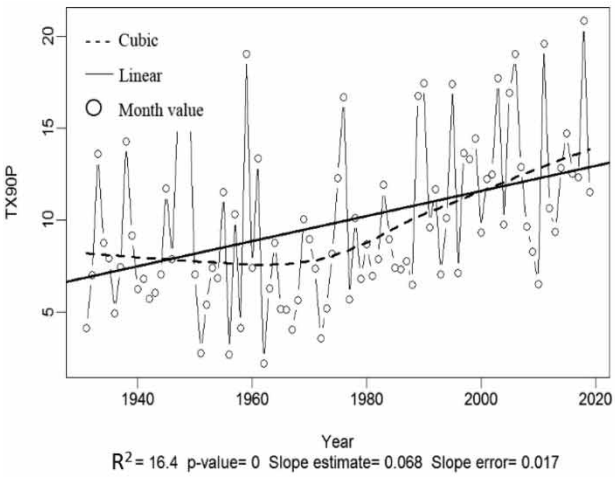

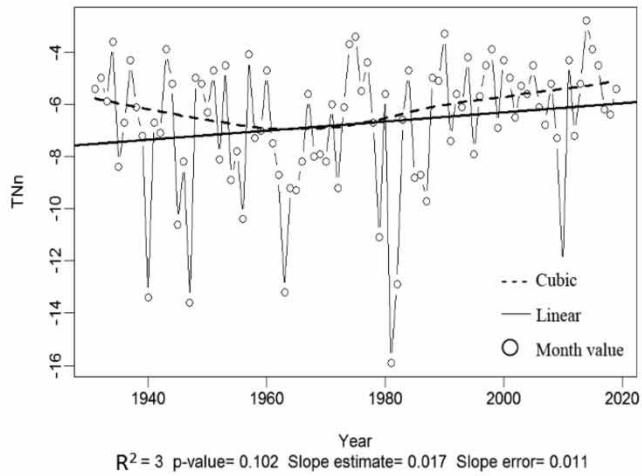

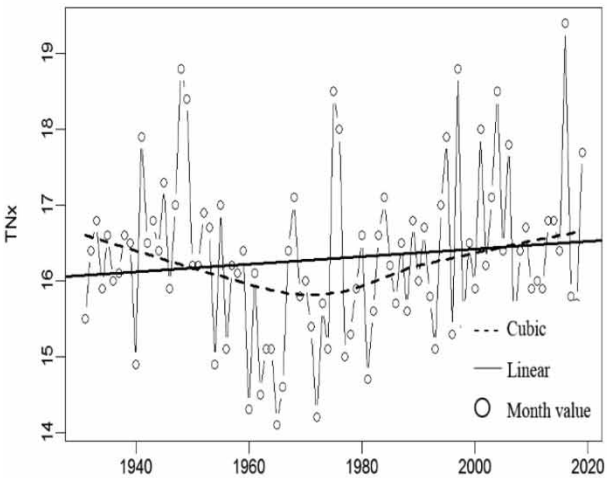

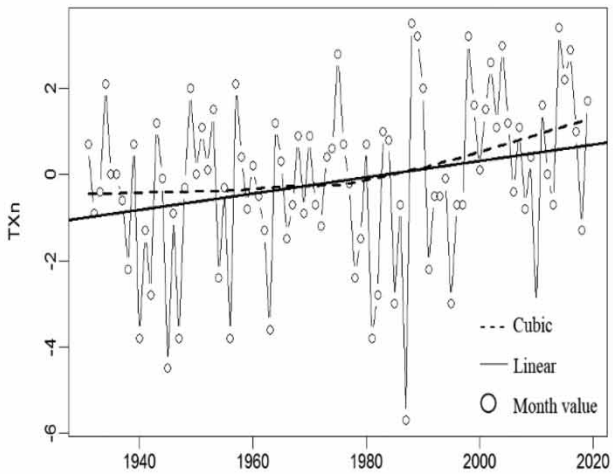

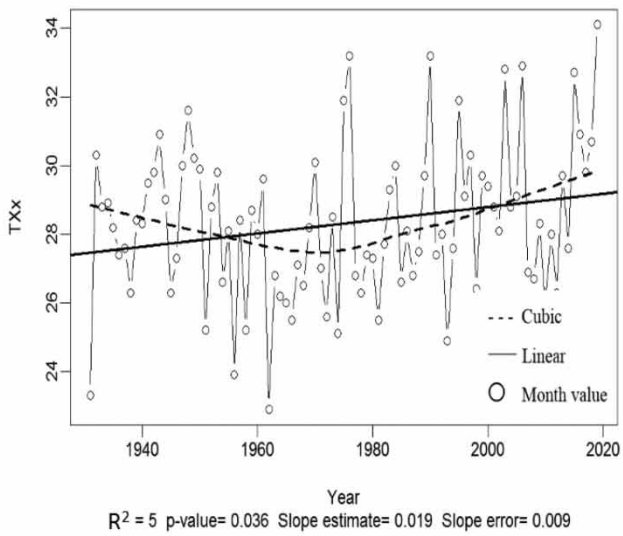

Figure 3 | Continued.

Meanwhile, the extreme indices of cool days and cool nights revealed a reduction in their values and a negative slope. It demonstrated an increase in temperatures in the study area. The extreme precipitation indices (RX1day and RX5day) depicted an increase with a slight slope (concerning a linear fit line). However, the cubic fit line slope showed a noticeable decline from 1985 onwards. This indicated that the study area is experiencing climate change and a reduction in extreme and significant precipitation. In Figure 3, circles that are significantly away from the standard deviation indicate extreme precipitation or temperatures. RX1day diagram, for illustration, shows three heavy 1-day precipitation from 2000 to 2019. Other studies have reported these anomalies in CE's precipitation and temperatures (Chapman *et al.* 2020; Kendon *et al.* 2020; Shi *et al.* 2021; Haupt & Fritsch 2022).

From Table 2, the Hurst exponent values of DTR, RX1day, RX5day, TN10p, TN90p, TX10p, and TX90p were delineated via a long-range correlation. These values revealed the long-term persistence of the previous state (in other words, an increase or reduction in values between two time steps are followed by an elevation or decline in the next step, respectively). The Hurst exponent was higher in TX10p than in other indices, suggesting a longer memory in its time series; meanwhile, DTR had the smallest $H(2)$, suggesting a less long-range correlation and more randomness in the time series. This indicated that variations of the extreme temperatures were more severe than those of precipitation. (This can be seen in Figure 3, where extreme precipitation indices are compared with extreme temperature indices.) Nonetheless, the TNn, TNx, TXn, and TXx time series possessed short memory or anti-persistence (in other words, an increase or reduction between two time steps can be followed by a decline or elevation in the next step). TNn exhibited the least anti-persistency, while TNx exhibited the highest. This suggested that long-term prediction of the extreme maximum and minimum daily temperatures in the study area is a complex exercise and possibly holds substantial errors.

The fluctuation function $F_q(s)$ considering several q values was estimated by means of the MF-DFA technique. Figure 4 illustrates the log-scaling of the qth $F_q(s)$ against s for q. It can be perceived from Figure 3 that the curves of all indices exhibited an increase in the time-scale range. This growth implies the multifractality of all indices in the time series. In other words, the scaling exponents' slope exhibits an extreme dependency on q values, indicating multifractal sources in the time series of extreme climate indices. Concerning DTR, TNn, TNx, TXn, and TXx, it is obvious that the scaling exponent of cross-correlations (crossover points) is in the proximity of 25 days, exhibiting scale variations at 25 days.

Figure 5 depicts the $H(q) \sim q$ diagrams (generalized fractal dimensions), $f(\alpha) \sim \alpha$ (singularity spectrum), and $\tau(q)$ against q (mass exponents) for the extreme climate indices. It is understood that the $H(q)$ nonlinear monotonically diminishes when faced with an increase in q values (Figure 5(a)). This indicates the multifractal behavior of all stations of the time series. Increased nonlinear behavior in the curves is indicative of increased multifractal features in the series. According to Figure 5(b), it is evident that with an escalation in q values, $\tau(q)$ rises as well. Ample multifractality was observed in the calculated indices. It should be considered that the supposed scale range for the calculation of DTR, TNn, TNx, TXn, and TXx $[2^3 \sim 2^{4.65}]$ was different from other indices $[2^3 \sim 2^{7.7}]$. Thus, the graphs of $H(q) \sim q$ (generalized fractal dimensions) and $\tau(q)$ against q (mass exponents) are dissimilar in the cases of DTR, TNn, TNx, TXn, and TXx and TX10p, TX90p, TN10p, TN90p,

Table 2 | Multifractal parameters of the time series of extreme climate indices

	$H(2)$	$\Delta\alpha$	ΔH
DTR	0.5012	1.9388	1.4142
RX1day	0.5817	0.3786	0.2382
RX5day	0.5685	0.2195	0.1273
TN10p	0.6308	0.4399	0.2858
TN90p	0.7318	0.3110	0.1912
TX10p	0.7524	0.6067	0.4395
TX90p	0.7038	0.5437	0.3741
TNn	0.4075	2.2437	1.6441
TNx	0.4830	2.039	1.4149
TXn	0.4360	1.9746	1.3678
TXx	0.4627	1.9378	1.3372

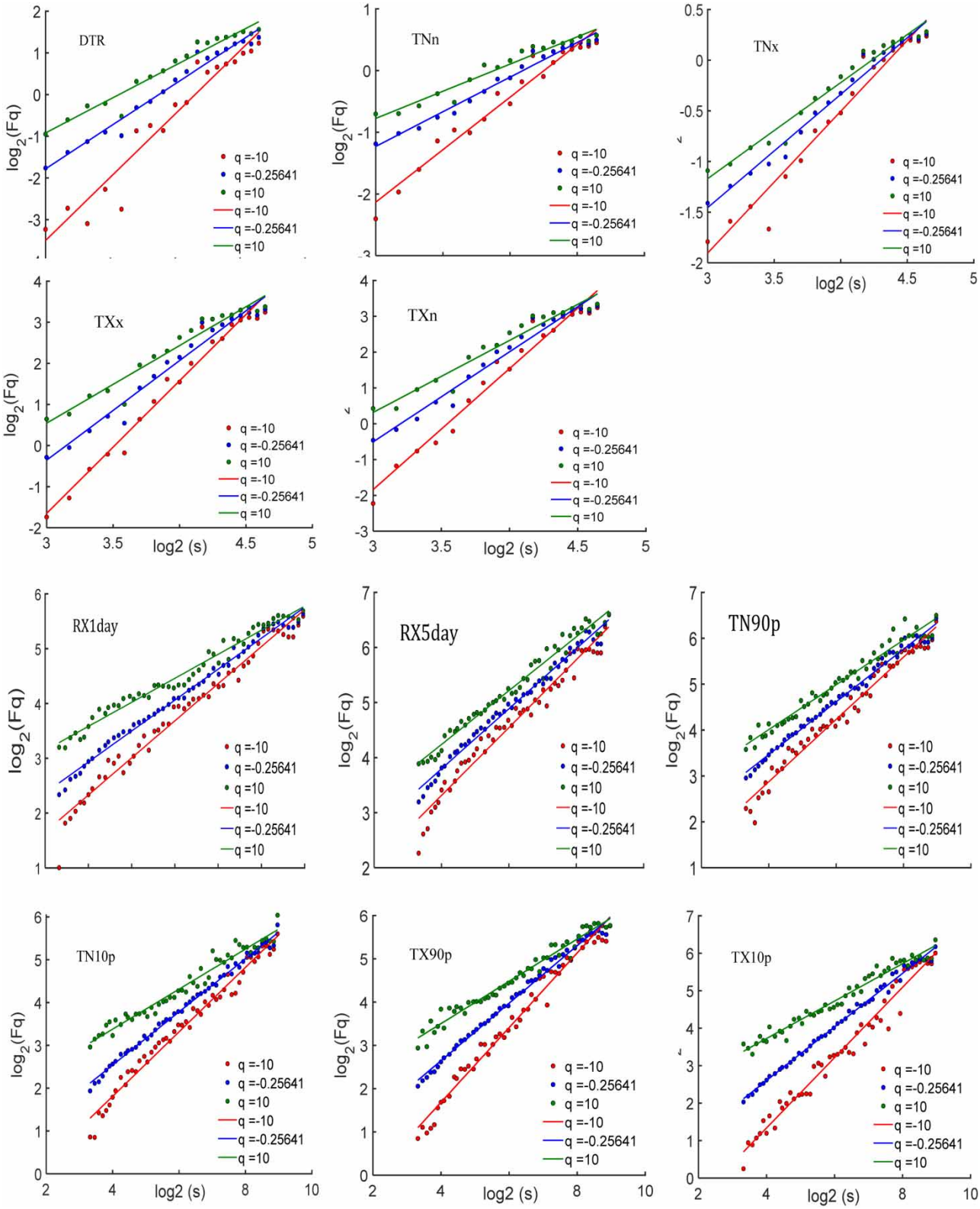

Figure 4 | Log-scaling graphs concerning the fluctuation function $F_q(s)$ against the time scale (s) of the extreme climate indices of CE.

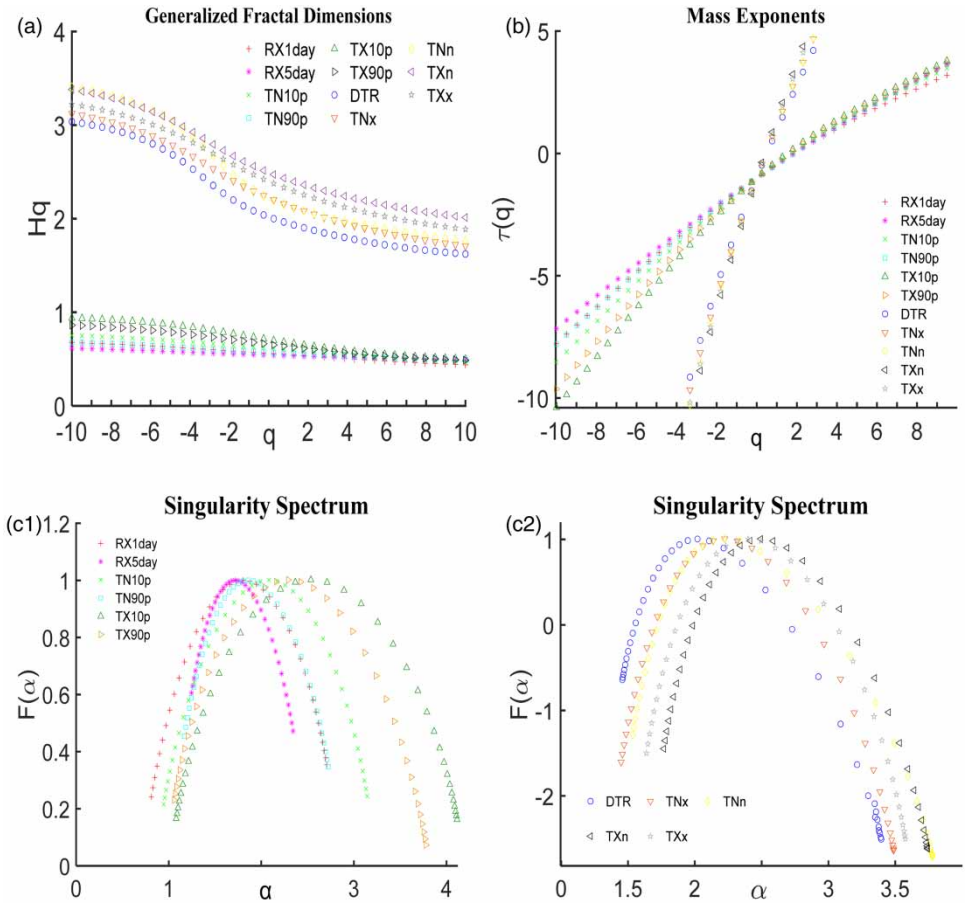

Figure 5 | The $H(q) \sim q$ (generalized fractal dimension) and $\tau(q) \sim q$ (mass exponents) curves ((a) and (b), respectively) and the singularity spectrum $f(\alpha) \sim \alpha$ ($(c-1, 2)$) of the extreme climate indices' time series for CE.

RX1day, and RX5day. Consequently, an analogy was drawn between extreme indices holding identical scale ranges. Extreme climate indices were divided into two categories: (1) DTR, TNn, TNx, TXn, and TXx possessed the scale range of $[2^3 \sim 2^{4.65}]$ and (2) TX10p, TX90p, TN10p, TN90p, RX1day, and RX5day held the scale range of $[2^3 \sim 2^{7.7}]$.

Concerning the second category, Figure 5(b) shows that the most meaningful nonlinear qualities are observed in TX10p, and the smallest proportions in RX5day, reflecting stronger and weaker multifractality in TX10p and RX5day, respectively. In respect of the first category, Figure 5(b) shows the utmost nonlinear qualities in DTR, and the least nonlinearity in TXn, indicating stronger and weaker multifractality in DTR and TXn, respectively. To confirm multifractality in the extreme climate indices' time series, and detect low and high fluctuation probabilities, the multifractal spectrum (Figure 5(c)) was depicted. As shown in Figure 5(c), the graphs of RX1day and TN10p showed left-side asymmetry. This approves multifractal properties of RX1day and TN10p, and indicates a high probability of low fluctuations. Moreover, it proves a lack of strong probability of the considerable number of cool nights and extreme 1-day precipitation in the study area. RX5day, DTR, TN90p, TX90p, TNn, TNx, TXn, and TXx all depicted right-side asymmetric curves, indicating a high probability of high fluctuations. Additionally, it establishes that extreme high temperature (warm days and warm nights) and extreme 5-day precipitation are expected in the study area. TX10p depicted a symmetrical curve, suggesting an equal probability of high and low fluctuations. Moreover, it testifies to a balanced number of cool nights in the study area.

To estimate the extreme climate indices' time-series multifractal strength, two multifractal parameters ($\Delta H(q)$ and $\Delta\alpha$) were identified and implemented, as shown in Table 2. Across the time series, the $\Delta H(q)$ values were highest for TX10p (in the second category; 0.4395) and TNx (in the first category; 1.6441), which implies that the multifractal features of TX10p and TNx were the most stimulating. RX5day (in the second category; 0.1273) and TXx (in the first category; 1.3372) registered the lowest $\Delta H(q)$ values, indicating more vulnerable multifractality. Meanwhile, $\Delta\alpha$ (the multifractal spectrum width)

Table 3 | The ΔH values of shuffled and surrogated time series of extreme climate indices

	Extreme climate indices					
First category	**TNn**	**TNx**	**TXn**	**TXx**	**DTR**	
$\Delta H_{\text{shuffled}}(q)$	0.5232	0.4087	0.6267	0.6478	0.7499	
$\Delta H_{\text{surrogated}}(q)$	1.5068	1.2731	1.5243	1.4974	1.2313	
Second category	**RX1day**	**RX5day**	**TN10p**	**TN90p**	**TX10p**	**TX90p**
$\Delta H_{\text{shuffled}}(q)$	0.2232	0.1846	0.2625	0.2532	0.2371	0.2532
$\Delta H_{\text{surrogated}}(q)$	0.2557	0.1472	0.1961	0.1877	0.3416	0.2566

measured the degree of multifractality within the time series. The larger the value of $\Delta\alpha$, the larger the variety in the time series; in other words, the greater the degree of multifractality, the more complexity can be observed in the data. Table 2 demonstrated that TX10p (in the second category; 0.6067) and TNx (in the first category; 2.2437) had the highest degrees of multifractality and complexity, respectively, while RX5day (in the second category; 0.2195) and TXx (in the first category; 1.9378) had the weakest, confirming the $\Delta H(q)$ results.

We found that all time series examined in this study possessed multifractal properties of varying strengths. Shuffling and surrogate methods were employed to investigate the dynamic causes of the multifractality of the extreme climate indices. Table 3 and Figure 6 indicate that the $H(q)_{\text{Shuf}}$ values of all indices were not equal to 0.5. The $\Delta H(q)$ values of the shuffled and surrogated time series DTR, TN10p, TNn, TNx, TX10p, TX90p, and TXn were lower than those of the original time series, indicating a reduction in multifractal strength. This suggests that the source of the multifractality of the time series was both correlation properties and PDF. The $\Delta H(q)$ values of RX1day, TXn, and TXx decreased with the shuffling of the time series but increased with surrogating, suggesting, again, that multifractal strength in the time series was the result of both correlation properties and PDF; however, the predominant source was correlation properties. The $\Delta H(q)$ value of TN90p increased with shuffling and decreased with surrogating, suggesting multifractality from both sources, but with PDF predominance. The $\Delta H(q)$ value of RX5day increased with shuffling and surrogating, demonstrating multifractal strength in the time series due to a balanced source of correlation properties and PDF.

The singularity spectrum $f(\alpha) \sim \alpha$ of shuffled and surrogated time series proved the previous results (in the case of multifractality sources in the extreme indices' time series) as well (see Figure 7).

The results verified that the multifractality source in the warm nights' behavioral patterns is PDF, while in the cases of lowest and highest maximum daily temperatures and maximum 1-day precipitation, it is the correlation properties. The time series of lowest and highest minimum daily temperatures, cool nights, cool days, warm days, and maximum 5-day precipitation are multifractal with both correlation properties and PDF sources. Accordingly, one can conclude that intra-study-

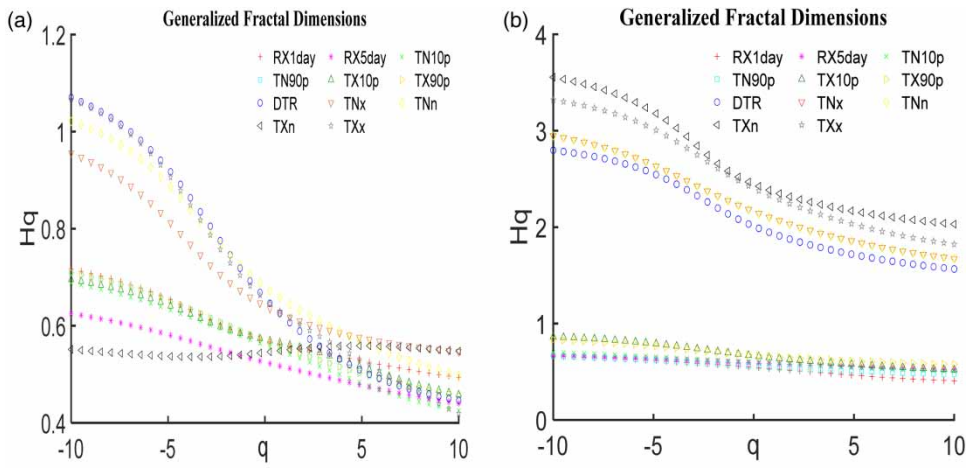

Figure 6 | The $H(q) \sim q$ (generalized fractal dimensions) curves of the shuffled (a) and surrogated (b) extreme climate indices' time series for CE.

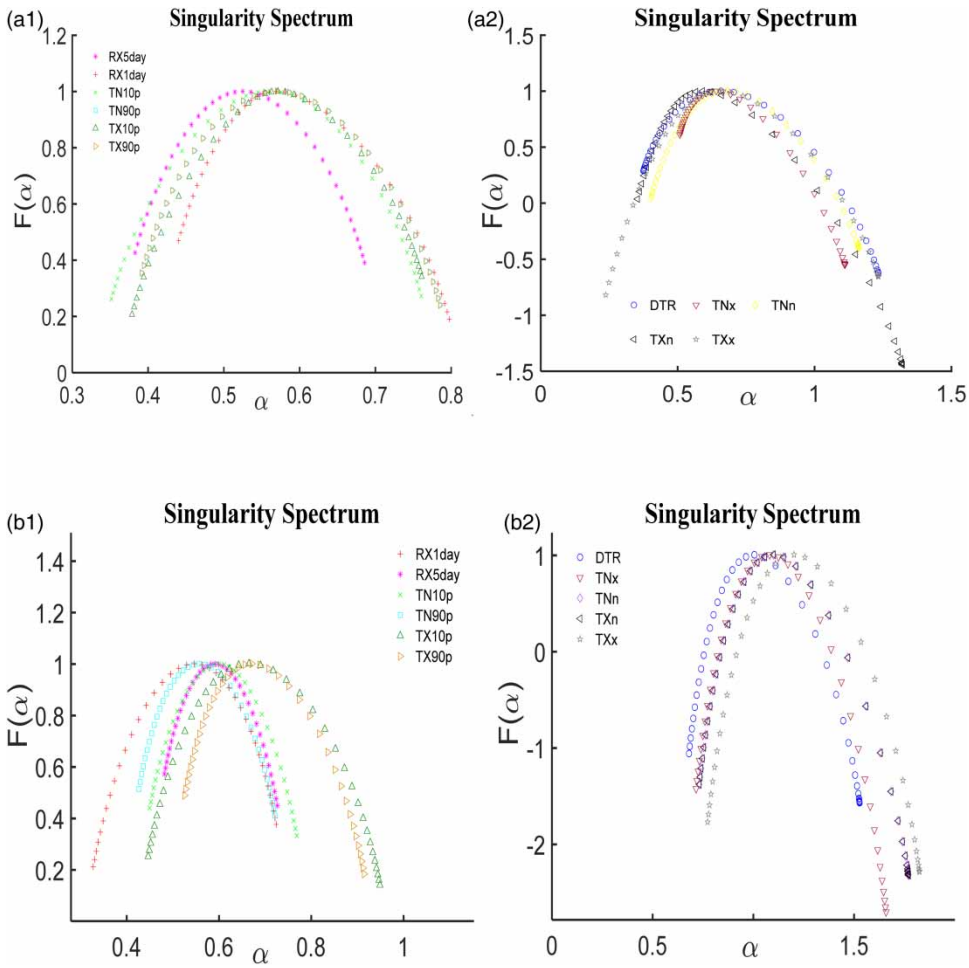

Figure 7 | The singularity spectrum $f(\alpha) \sim \alpha$ ((c)) of shuffled (a) and surrogated (b) time series of extreme indices for CE.

area factors can affect multifractal patterns governing lowest and highest maximum daily temperatures and maximum 1-day precipitation. Meanwhile, multifractal patterns of lowest and highest minimum daily temperatures, cool nights, cool days, warm days, and maximum 5-day precipitation were relatively independent of intra-study-area factors.

Summarizing the results, the study of shifts in extreme climate indices emphasized climate change in the study area (CE). Behavioral patterns of maximum 1-day and 5-day precipitation, cool and warm nights, cool and warm days, maximum and minimum of maximum daily temperature, maximum and minimum of minimum daily temperature, and DTR were multifractal. Even though the multifractal source of the warm nights was PDF, the multifractal source of the minimum and maximum of maximum daily temperature and maximum 1-day precipitation was correlation properties. The sources of multifractal behavioral patterns of maximum and minimum of minimum daily temperature, cool nights, cool and warm days, and maximum 5-day precipitation were both correlation properties and PDF.

de Souza *et al.* (2013) and Berkes *et al.* (2009) investigated multifractal patterns in temperature series regarding CE. They drew two general conclusions. (1) They discovered the climatic change in the study area by examining anomalies in the temperature time series. (2) They found that the multifractal properties of the temperature time series are due to linear and nonlinear dependencies in dynamics and a small contribution of deviation from the Gaussianity. In other words, the sources of the multifractality of the temperature series were both correlation properties and PDF, supporting the findings of the present study concerning temperature. However, their study had limitations, and their results did not sufficiently provide evidence for the existence of multifractal patterns in extreme precipitation and temperatures. The limitations include:

- Failure to study extreme temperature multifractal patterns and their sources.

To cite two examples: failure to study the maximum Tmin and minimum Tmin multifractal patterns and their sources.

• Failure to study extreme precipitation multifractal patterns and their sources.

Further studies, such as Chapman *et al.* (2020), Kendon *et al.* (2020), Shi *et al.* (2021), and Haupt & Fritsch (2022), examined trends and variations in temperature and precipitation in CE from non-dynamic perspectives. Nevertheless, they ignored the study of nonlinear dynamic patterns (multifractal) governing extreme precipitation and temperatures as well as their sources. To the best of the authors' knowledge, to date, no study has evaluated extreme 1-day and 5-day precipitations' multifractal patterns and their sources. Hence, this study is of relevance because it covers the information gaps in the previous studies. Investigating climate change in the study area (CE) by considering multifractal properties of extreme climate indices is beyond the scope of this study. Accordingly, this issue can be explored in future studies.

5. CONCLUSIONS

This study revealed the multifractal patterns of extreme temperatures and precipitation in CE to determine the embedded fractal mechanism in the extremes. The study is of relevance because it examines precipitation and temperature patterns, which are of significance to managing water resources and assessing the risks of floods and droughts. To achieve the objectives, we employed 11 extreme climate indices to create an overview of the extremes in temperature and precipitation series. Then, we used the MF-DFA method, shuffling, and surrogating methods to study the multifractality sources of the time series. The results indicated that all the indices' time series were multifractal. Moreover, the observed multifractal strength was the product of both correlation properties (long-range correlations between small and large fluctuations) and PDF. The nonlinear dynamic patterns in the maximum 1-day precipitation amount, minimum of maximum temperature, and maximum of maximum temperature were predominantly produced by correlation properties, whereas the nonlinear dynamic patterns in the warm nights were due to a PDF predominance. Besides, nonlinear dynamic patterns governing the DTR, maximum 5-day precipitation, maximum of minimum temperature, minimum of minimum temperature, cool nights, cool days, and warm days were produced by the identical extent of correlation properties and the PDF. The intra-study-area factors can affect multifractal patterns governing lowest and highest maximum daily temperatures and maximum 1-day precipitation. Meanwhile, multifractal patterns of lowest and highest minimum daily temperatures, cool nights, cool days, warm days, and maximum 5-day precipitation were relatively independent of intra-study-area factors.

FUNDING

This research did not receive any specific grant from funding agencies in the public, commercial, or not-for-profit sectors.

AUTHORS' CONTRIBUTIONS

F.R. conceptualized the original draft, did formal analysis, and investigated and wrote the preparation of original draft. F.R. and M.H.F. were involved in devising the methodology, wrote (reviewed and edited) the original draft and supervised.

CONFLICTS OF INTEREST

The authors have no conflict of interest to declare.

DATA AVAILABILITY STATEMENT

The precipitation and temperatures data are available at: https://www.metoffice.gov.uk/hadobs/hadcet/data/download.html and https://www.metoffice.gov.uk/hadobs/hadukp/.

REFERENCES

Abbasnia, M. & Toros, H. 2019 Analysis of long-term changes in extreme climatic indices: a case study of the Mediterranean climate, Marmara Region, Turkey. In: *Meteorology and Climatology of the Mediterranean and Black Seas*. Birkhäuser, Cham, pp. 141–153. https://doi.org/10.1007/978-3-030-11958-4_9.

Adarsh, S., Nourani, V., Archana, D. S. & Dharan, D. S. 2020 Multifractal description of daily rainfall fields over India. *Journal of Hydrology* **586**, 124913. https://doi.org/10.1016/j.jhydrol.2020.124913.

Agbazo, M., N'Gobi, G. K., Alamou, E., Kounouhewa, B. & Afouda, A. 2019 Detection of hydrological impacts of climate change in Benin by a multifractal approach. *International Journal of Water Resources and Environmental Engineering* **11** (2), 45–55. https://doi.org/10.5897/IJWREE2018.0819.

Alexander, L. V. & Jones, P. D. 2001 Updated precipitation series for the U.K. and discussion of recent extremes. *Atmospheric Science Letter* **1** (2), 115–124. https://doi.org/10.1006/asle.2001.0025.

Alexander, L. V., Zhang, X., Peterson, T. C., Caesar, J., Gleason, B., Klein Tank, A. M. G., Haylock, M., Collins, D., Trewin, B., Rahimzadeh, F. & Tagipour, A. 2006 Global observed changes in daily climate extremes of temperature and precipitation. *Journal of Geophysical Research: Atmospheres* **111** (D5). https://doi.org/10.1029/2005JD006290

Asadullah, A. 2019 "Floods are fascinating and miserable" and other things we can all agree on. The UK experience of academia, industry and government working together in flood hydrology. In: *Geophysical Research Abstracts (Vol. 21)*, EGU General Assembly 2019, 7–12 April 2019, Vienna, Austria. EGU, Munich, Germany.

Berkes, I., Gabrys, R., Horváth, L. & Kokoszka, P. 2009 Detecting changes in the mean of functional observations. *Journal of the Royal Statistical Society: Series B (Statistical Methodology)* **71** (5), 927–946. https://doi.org/10.1111/j.1467-9868.2009.00713.x.

Brown, G., Michon, G. & Peyrière, J. 1992 On the multifractal analysis of measures. *Journal of Statistical Physics* **66** (3), 775–790. https://doi.org/10.1007/BF01055700.

Bryan, K., Ward, S., Roberts, L., White, M. P., Landeg, O., Taylor, T. & McEwen, L. 2020 The health and well-being effects of drought: assessing multi-stakeholder perspectives through narratives from the UK. *Climatic Change* **163** (4), 2073–2095. https://doi.org/10.1007/s10584-020-02916-x.

Chapman, S. C., Murphy, E. J., Stainforth, D. A. & Watkins, N. W. 2020 Trends in winter warm spells in the central England temperature record. *Journal of Applied Meteorology and Climatology* **59** (6), 1069–1076. https://doi.org/10.1175/JAMC-D-19-0267.1.

de Souza, J., Duarte Queiros, S. M. & Grimm, A. M. 2013 Components of multifractality in the central England temperature anomaly series. *Chaos: An Interdisciplinary Journal of Nonlinear Science* **23** (2), 023130. https://doi.org/10.1063/1.4811546.

Doe, R. K. 2004 Extreme precipitation and run-off induced flash flooding at Boscastle, Cornwall, UK, 16 August 2004. *Journal of Meteorology-Trowbridge Then Bradford on Avon* **29**, 319–333.

Espen Ihlen 2020 *Multifractal Detrended Fluctuation Analysis*. MATLAB Central File Exchange. Available from: https://www.mathworks.com/matlabcentral/fileexchange/38262-multifractal-detrended-fluctuation-analyses (accessed 17 December 2020).

Evertsz, C. J. & Mandelbrot, B. B. 1992 Multifractal measures. *Chaos and Fractals* **1992**, 921–953.

Feder, J. 1988 *Fractals*. Plenum Press, New York, NY. Available from: https://www.abebooks.com/servlet/BookDetailsPL?bi=30419426371&searchurl=an%3Djens%2Bfeder%26sortby%3D17%26tn%3Dfractals&cm_sp=snippet-_-srp1-_-title1 (accessed 20 Mar 2018).

Frisch, U. & Parisi, G. 1985 Fully developed turbulence and intermittency. In: *Turbulence and Predictability in Geophysical Fluid Dynamics and Climate Dynamics* (Ghil, M., Benzi, R. & Parisi, G., eds.). North-Holland, New York, pp. 84–88.

Ge, E. & Leung, Y. 2013 Detection of crossover time scales in multifractal detrended fluctuation analysis. *Journal of Geographical Systems* **15** (2), 115–147. https://doi.org/10.1007/s10109-012-0169-9.

Golding, B., Clark, P. & May, B. 2005 The Boscastle flood: meteorological analysis of the conditions leading to flooding on 16 August 2004. *Weather* **60** (8), 230–235. https://doi.org/10.1256/wea.71.05.

Guo, E., Zhang, J., Wang, Y., Quan, L., Zhang, R., Zhang, F. & Zhou, M. 2019 Spatiotemporal variations of extreme climate events in Northeast China during 1960–2014. *Ecological Indicators* **96**, 669–683. https://doi.org/10.1016/j.ecolind.2018.09.034.

Hao, W., Shao, Q., Hao, Z., Ju, Q., Baima, W. & Zhang, D. 2019 Non-stationary modelling of extreme precipitation by climate indices during rainy season in Hanjiang River Basin, China. *International Journal of Climatology* **39** (10), 4154–4169. https://doi.org/10.1002/joc.6065.

Haupt, H. & Fritsch, M. 2022 Quantile trend regression and its application to central England temperature. *Mathematics* **10** (3), 413. https://doi.org/10.3390/math10030413.

Hekmatzadeh, A. A., Torabi Haghighi, A., Hosseini Guyomi, K., Amiri, S. M. & Kløve, B. 2020 The effects of extremes and temporal scale on multifractal properties of river flow time series. *River Research and Applications* **36** (1), 171–182. https://doi.org/10.1002/rra.3550.

Holman, I. P., Hess, T. M., Rey, D. & Knox, J. W. 2021 A multi-level framework for adaptation to drought within temperate agriculture. *Frontiers in Environmental Science* **8**, 282. https://doi.org/10.3389/fenvs.2020.589871.

Isaacson, L. K. 2018 Entropy generation through the interaction of laminar boundary-layer flows: sensitivity to initial conditions. *Journal of Modern Physics* **9** (08), 1660.

Kantelhardt, J. W., Zschiegner, S. A., Koscielny-Bunde, E., Havlin, S., Bunde, A. & Stanley, H. E. 2002 Multifractal detrended fluctuation analysis of nonstationary time series. *Physica A: Statistical Mechanics and its Applications* **316** (1–4), 87–114. https://doi.org/10.1016/S0378-4371(02)01383-3.

Kantelhardt, W. J., Rybski, D., Zschiegner, S. A., Braun, P., Koscielny-Bunde, E., Livina, V., Havlin, S. & Bunde, A. 2003 Multifractality of river runoff and precipitation: comparison of fluctuation analysis and wavelet methods. *Physica A: Statistical Mechanics and its Applications* **330** (1), 240–245. https://doi.org/10.1016/j.physa.2003.08.019.

Kendon, M., McCarthy, M., Jevrejeva, S., Matthews, A., Sparks, T. & Garforth, J. 2020 State of the UK Climate 2019. *International Journal of Climatology* **40**, 1–69. https://doi.org/10.1002/joc.6726.

Liu, Y. H., Zhang, K. X., Zhang, W. C., Shao, Y. H., Pei, H. Q. & Feng, J. M. 2013 Multifractal analysis of 1-min summer rainfall time series from a monsoonal watershed in eastern China. *Theoretical and Applied Climatology* **111**, 37–50.

Mandelbrot, B. B. 1989 Multifractal measures, especially for the geophysicist. In: *Fractals in Geophysics*. Birkhäuser, Basel, pp. 5–42. https://doi.org/10.1007/978-3-0348-6389-6_2.

Mandelbrot, B. B. 1982 *The Fractal Geometry of Nature*, Vol. 1. W.H. Freeman, New York.

Mandelbrot, B. B., Fisher, A. J. & Calvet, L. E. 1997 *A Multifractal Model of Asset Returns*. Available from SSRN: https://ssrn.com/abstract=78588 (accessed 22 Mar 2020).

Marsh, T. J. 2001 The 2000/2001 floods in the UK – a brief overview. *Weather* **56**, 343–345. https://doi.org/10.1002/j.1477-8696.2001.tb06506.x.

Miloş, L. R., Haţiegan, C., Miloş, M. C., Barna, F. M. & Boţoc, C. 2020 Multifractal detrended fluctuation analysis (MF-DFA) of stock market indexes. Empirical evidence from seven central and eastern European markets. *Sustainability* **12** (2), 535. https://doi.org/10.3390/su12020535.

Movahed, M. S., Jafari, G. R., Ghasemi, F., Rahvar, S. & Tabar, M. R. R. 2006 Multifractal detrended fluctuation analysis of sunspot time series. *Journal of Statistical Mechanics: Theory and Experiment* **2006** (02), P02003. https://doi.org/10.1088/1742-5468/2006/02/P02003.

Muzy, J. F., Bacry, E. & Arneodo, A. 1991 Wavelets and multifractal formalism for singular signals: application to turbulence data. *Physical Review Letters* **67** (25), 3515. https://doi.org/10.1103/PhysRevLett.67.3515.

Olsen, L. 1995 A multifractal formalism. *Advances in Mathematics* **116** (1), 82–196. https://doi.org/10.1006/aima.1995.1066.

Panthou, G., Vischel, T. & Lebel, T. 2014 Recent trends in the regime of extreme rainfall in the Central Sahel. *International Journal of Climatology* **34** (15), 3998–4006. https://doi.org/10.1002/joc.3984.

Parker, D. E., Legg, T. P. & Folland, C. K. 1992 A new daily central England temperature series, 1772–1991. *International Journal of Climatology* **12** (4), 317–342.

Parsons, D. J., Rey, D., Tanguy, M. & Holman, I. P. 2019 Regional variations in the link between drought indices and reported agricultural impacts of drought. *Agricultural Systems* **173**, 119–129. https://doi.org/10.1016/j.agsy.2019.02.015.

Peng, C. K., Buldyrev, S. V., Havlin, S., Simons, M., Stanley, H. E. & Goldberger, A. L. 1994 Mosaic organization of DNA nucleotides. *Physical Review E* **49** (2), 1685. https://doi.org/10.1103/PhysRevE.49.1685.

Pesin, Y. B. 2008 *Dimension Theory in Dynamical Systems*. University of Chicago Press, Chicago, IL.

Rahmani, F. & Fattahi, M. H. 2021a A multifractal cross-correlation investigation into sensitivity and dependence of meteorological and hydrological droughts on precipitation and temperature. *Natural Hazards*, 1–23. https://doi.org/10.1007/s11069-021-04916-1.

Rahmani, F. & Fattahi, M. H. 2021b Nonlinear dynamic analysis of the fault activities induced by groundwater level variations. *Groundwater for Sustainable Development*, 100629. https://doi.org/10.1016/j.gsd.2021.100629.

Rahmani, F. & Fattahi, M. H. 2021c Phase space mapping of pivotal climatic and non-climatic elements affecting basin' drought. *Arabian Journal of Geosciences* **14** (5), 1–12. https://doi.org/10.1007/s12517-021-06734-y.

Rego, C. R. C., Frota, H. O. & Gusmão, M. S. 2013 Multifractality of Brazilian rivers. *Journal of Hydrology* **495**, 208–215. http://dx.doi.org/10.1016/j.jhydrol.2013.04.046.

Renard, B. & Thyer, M. 2019 Revealing hidden climate indices from the occurrence of hydrologic extremes. *Water Resources Research* **55** (9), 7662–7681. https://doi.org/10.1029/2019WR024951.

Riedi, R. 1995 An improved multifractal formalism and self-similar measures. *Journal of Mathematical Analysis and Applications* **189** (2), 462–490. https://doi.org/10.1006/jmaa.1995.1030.

Schreiber, T. & Schmitz, A. 1996 Improved surrogate data for nonlinearity tests. *Physical Review Letters* **77** (4), 635. https://doi.org/10.1103/PhysRevLett.77.635.

Schreiber, T. & Schmitz, A. 2000 Surrogate time series. *Physica D: Nonlinear Phenomena* **142** (3–4), 346–382. https://doi.org/10.1016/S0167-2789(00)00043-9.

Seo, S. B., Kim, Y. O., Kim, Y. & Eum, H. I. 2019 Selecting climate change scenarios for regional hydrologic impact studies based on climate extremes indices. *Climate Dynamics* **52** (3), 1595–1611. https://doi.org/10.1007/s00382-018-4210-7.

Shi, X., Beaulieu, C., Killick, R. & Lund, R. 2021 Changepoint Detection: An Analysis of the Central England Temperature Series. *arXiv preprint arXiv:2106.12180*. https://arxiv.org/abs/2106.12180.

Singh, V. & Qin, X. 2020 Study of rainfall variabilities in Southeast Asia using long-term gridded rainfall and its substantiation through global climate indices. *Journal of Hydrology* **585**, 124320. https://doi.org/10.1016/j.jhydrol.2019.124320.

Vega, A. J. & Rohli, R. V. 2012 *Climatology*, 3rd edn. Jones & Bartlett Learning, Burlington, MA, p. 444.

Wallace, E. 2022 Quantifying and modelling spatio-temporal flood-mitigation, drought-resilience, and water-quality benefits provided by grassland interventions in the Eden Catchment (North-West England, UK). Doctoral dissertation, Lancaster University, Lancaster, UK.

Wang, Y., Zhang, Q. & Singh, V. P. 2016 Spatiotemporal patterns of precipitation regimes in the Huai River basin, China, and possible relations with ENSO events. *Natural Hazards* **82** (3), 2167–2185. https://doi.org/10.1007/s11069-016-2303-3.

Wheater, H. S. 2006 Flood hazard and management: a UK perspective. *Philosophical Transactions of the Royal Society A: Mathematical, Physical and Engineering Sciences* **364** (1845), 2135–2145. https://doi.org/10.1098/rsta.2006.1817

Zhang, X., Zhang, G., Qiu, L., Zhang, B., Sun, Y., Gui, Z. & Zhang, Q. 2019 A modified multifractal detrended fluctuation analysis (MFDFA) approach for multifractal analysis of precipitation in dongting lake basin, China. *Water* **11** (5), 891. https://doi.org/10.3390/w11050891.

First received 15 December 2021; accepted in revised form 15 March 2022. Available online 28 March 2022